1 *Article*

2 # CFD analysis of twin turbulent impinging

3 # axisymmetric jets at different impingement angles

4

5 **Raj Narayan Gopalakrishnan [1] and Dr. Peter J Disimile [2]**

6 [1] Department of Aerospace Engineering, University of Cincinnati, Cincinnati, OH, USA 45221;
7   gopalara@mail.uc.edu
8 [2] Department of Aerospace Engineering, University of Cincinnati, Cincinnati, OH, USA 45221;
9   peter.disimile@uc.edu
10 * Correspondence: gopalara@mail.uc.edu

11

12 **Abstract:** Based on the insight gained from single jet analysis performed earlier [1], CFD analysis on
13 turbulent jets impinging on one another at an angle was performed. Multiple impingement angles
14 were considered for this study to gain better understanding of the parameters affecting resultant jet
15 growth and velocity distribution. From the study of single jet, it was concluded that the SST k-ω
16 turbulence model was the ideal turbulence model capable of accurately predicting the flow physics
17 of the jets exiting a fully developed pipe at low Reynolds number. Hence, for the study of impinging
18 jets, SST k-ω turbulence model was used to study the velocity and jet growth characteristics. It
19 became evident that the mesh alignment with the velocity vector at exit of the pipe domain plays a
20 crucial role in the accuracy of the results. The parameter used to evaluate this condition was
21 identified as False Diffusion and was observed to affect the TKE parameter significantly. Methods
22 to reduce false diffusion are also discussed in this article. Based on the mesh obtained from the grid
23 sensitivity study, jets impinging at 30, 45 and 60 degrees at Reynolds number of 7500 were
24 numerically analyzed. It was observed that the profile of the resultant jet closely matched with the
25 prediction of elliptical profile predicted by past researchers, [2] and [3]. Also, it was seen that higher
26 jet growth was predicted in case of jets impinging at a higher impingement angle.

27 **Keywords:** Reynolds-averaged Navier–Stokes (RANS), Round Jets, Turbulence Model, Impinging
28 jets, SST k-omega model

29

30 **1. Introduction**

31   Impinging jets has large number of industrial applications since it is capable of enhancing fluid
32 mixing and increasing the spread rate of the resultant jet. The application of impinging jets has been
33 found in space propulsion rocket fuel-oxidizer mixing chamber, in internal combustion engines and
34 in spray generation. The team at ESI (Engineering & Scientific Innovations, Inc) is currently looking
35 at establishing the use of impinging jets as mechanism for fire suppressant discharge.
36   The fuel-oxidizer injector plate used in F-1 rocket engine of Saturn V rocket, along with the cross
37 section of injector plate and modes of impingement is shown in Figure 1 [4].
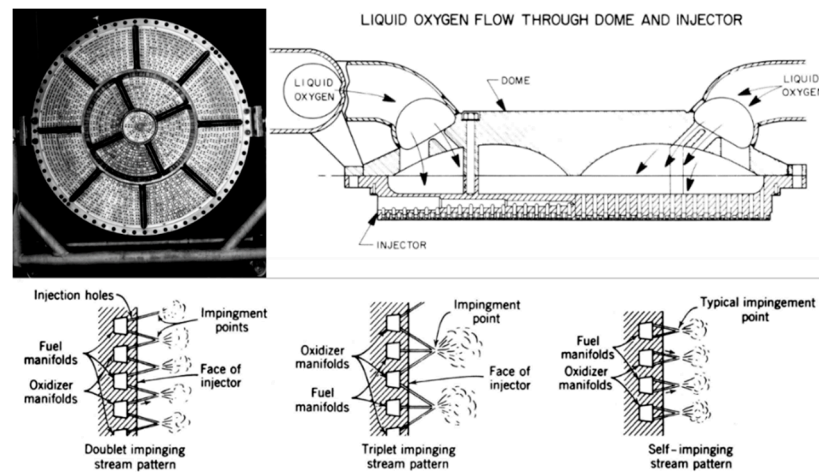
Figure 1. Injector plate used in F-1 rocket engine and modes of jet impingement used

The work done by Disimile et al. [2] has provided insight into the spread characteristics of the resultant jet after impingement at constant Reynolds number of 7500. They studied the round impinging jets at 2 angles; 30 and 45 degrees. From their study, it was observed that the growth characteristics of the resultant jet along plane normal to impingement plane for 45-degree impingement case was approximately 50% greater than the 30-degree impingement case. They also observed an elliptical profile for the resultant jet, similar to the observation made by Rho et al. [3] with major axis of the ellipse being 2.5 times greater than the minor axis in case of 45-degree impingement configuration and 1.6 times the minor axis for the 30-degree impingement case. The significant difference in growth along the major axis when compared with minor axis for two different impingement angles is an indicator of its effect on the resultant jet characteristics.

Rho et al. [3] performed an experimental study on cross jet mixing flows exiting nozzle condition. They considered circular nozzles and an impingement angle of 45-degrees for their study. The Reynolds number considered for the case under study was 52,000 and 65,000. They also observed an elliptical profile for the resultant jet after impingement, which has consistently been noted by other researchers. The shape of the resultant jet was observed to shift from an elliptical to circular profile further downstream. It was also concluded that, beyond the impingement zone; the mean velocity profile can be correlated to semi-empirical equations based on jet half-width.

Landers and Disimile [5] [6] [7] [8] has done significant amount of research on the near field of single jets, which were used as the baseline case for their work on impinging jets. Landers [9] congregated the results from the above-mentioned studies into his thesis based on the experimental analysis performed on impinging jets at various angles. Hence, for the current study; experimental data from Landers [9] is used for the validation of results obtained from CFD analysis to ensure reasonable agreement.

Prof. N. Rajaratnam of University of Alberta has performed significant research on topics related to turbulent jets in general and impinging jets in particular. His book on turbulent jets [10] has been an ideal technical source for the single jet study. Rajaratnam and Khan [11] studied impinging jets at 4 different angles (30, 60, 90 and 120-degrees) at Reynolds number of 30,000. They established the physics of the flow based on 2 regions; a zone from nozzle exit to impingement point, and a zone beyond impingement point. Detailed observations related to pressure and velocity characteristics were made in these regions for analysis. They observed that beyond the impingement point, the growth of the jet in the plane normal to the plane of nozzles was thrice the growth observed along the plane of nozzles. Also, as they moved further downstream, the flow tended to become axisymmetric with growth rate persisting at 1.5 times the growth rate for single round jet.

Rajaratnam and Wu [12] performed experimental study on impinging jets at 60-degree angle with unequal momentum. They considered incompressible flows with different velocities exiting each of the nozzle. The value of velocities studied ranged from 0 to 42 m/s and the ratio of velocities considered were 0.39, 0.47, 0.59, 0.68 and 0.79. Hence, none of their testing considered symmetric

78 profile. Similar to [11], the physics of the flow was established based on the location with respect to
79 impingement point. Beyond impingement point, they observed that the resultant jet axis can be
80 predicted using momentum considerations. They observed that the growth of the jet in plane of the
81 nozzle did not significantly depend on the velocity ratio. But along the plane normal to the plane of
82 nozzle, they were able to establish direct correlation between the velocity ratio and growth profile.
83 Similar to the observation made in [11], the growth of the combined jet in the plane normal to the
84 plane of nozzles was significantly more than the growth in the plane of the nozzles.
85   Elangovan et al. [13] presented their work on interaction of twin intersecting axisymmetric
86 turbulent jets at low Mach numbers (0.2). The exit diameter of the nozzles was 10 mm each and the
87 spacing between the centerlines of the nozzles was 31 mm with impingement angles considered being
88 0, 10, 20 and 30-degrees. They established 3 zones based on jet interactions as shown in Figure 2 –
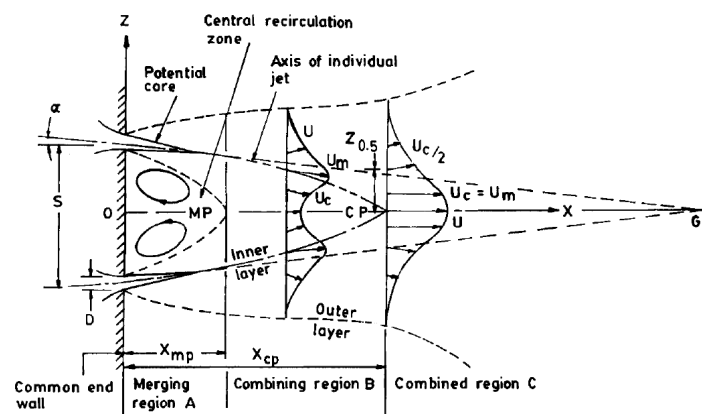89 merging region, combining region and combined region.
90

Figure 2. Notation of flow field used by Elangovan [1996]

94   As seen in Figure 2, significant recirculation occurs in the merging region with ambient flow
95 entrainment into the free shear layers of jets. At the Merging Point (MP), the free shear layers of
96 individual jet interact with one another. Combining region was defined as the zone beyond MP
97 extending up to the location where the centerline velocity becomes maximum. This location was
98 defined as Combining Point (CP). Beyond CP, the region was characterized by the resultant jet
99 resembling a single jet flow. Hence, this region was suitably named combined region were GP
100 represents the meeting of the geometric centerlines of each nozzle.
101   They observed that the near field flow physics was strongly dependent on the impingement
102 angle, and that the resultant flow field downstream of combining point resembled elliptic profile.
103 They also observed the axis-switching characteristics which is considered a phenomenon closely
104 associated with non-circular jets. Like previous researchers, they observed that the growth of the
105 resultant jets in the plane normal to nozzle plane was significantly higher than growth in nozzle
106 plane. Regarding the entrainment of the ambient fluid into the jet shear layer, they observed that the
107 entrainment was higher at lower angle, with maximum being at 0 degrees and consistently reduced
108 with increasing impingement angle. Similarly, the team [14] has studied the effect of impingement
109 angle and distance between nozzles centers for sonic and supersonic conditions.
110   An observation made by Landers [9] that seems to be very astute is that only limited amount of
111 published research work has been observed for impinging jets, either computational or experimental.
112 Most of the published results available are very application-specific and mainly dealing with
113 supersonic flows. Hence, obtaining well established data set for validation has proven quite difficult
114 for the case under consideration. Considering the ubiquitous nature of impinging jets in industrial
115 applications, we can only conclude that the results, if any, has not been tabulated or published either
116 because of sensitive nature of application (such as spacecraft propulsion fuel mixing, defense-related
117 study) or because of proprietary nature (such as impinging jets in combustion chambers of engines,
118 spray formation systems). Hence, it was considered very significant to establish one of the initial

119 works on impinging jets at low Reynolds number involving both computational and experimental
120 side.

2. Computational Methodology

122   The current study is performed based on the insight gained from the analysis of single turbulent
123 round jet (as discussed in [1]) at low Reynolds number (Re) of 7500. In the case of single jet study, the
124 inlet boundary condition was modelled as exiting from a fully developed pipe into ambient
125 conditions. In order to obtain the velocity and Turbulent Kinetic Energy (TKE) profile of fully
126 developed pipe, it was decided that the pipe flow be modelled separately and the profile from the
127 pipe flow simulation used as the inlet condition for jet. The results from the study of single round jets
128 were closely validated with experimental data which provided confidence that the strategy used was
129 accurate. Hence, the same strategy was used in the case of impinging jet study. For the study of
130 impinging jets, the full model generated is shown in Figure 3. The pipe sections were analyzed first,
131 followed by impinging jet domain. This methodology has successfully helped in reducing the
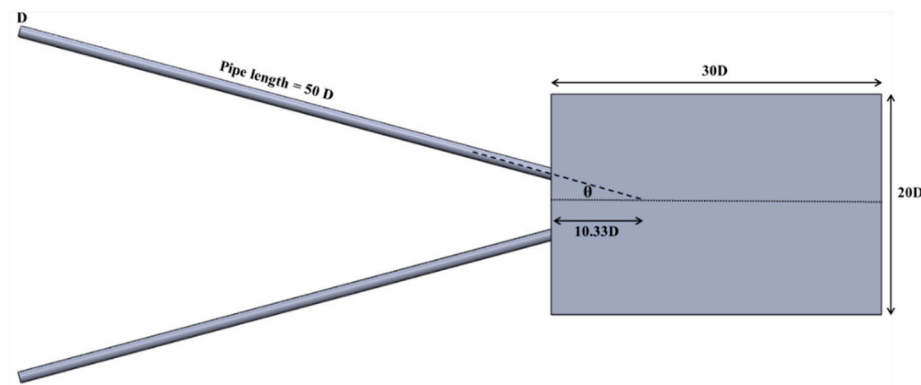132 computational requirements since the cases were treated separately.

Figure 3. Schematic of full geometry

3. Geometry and Mesh Generation

137   As discussed earlier, the full geometry was initially modelled as a pipe and ambient domain. It
138 was designed as a pipe with diameter D, length 50D exiting into ambient air (at standard pressure
139 and temperature) domain with length of 30D and height and width parameter being 20D each. The
140 pipes are inclined at an angle of θ to the central plane, which is termed as the Half Impingement
141 Angle (HIA). In the current study, the HIA considered are 15o, 22.5o and 30o. The mesh for the
142 inclined pipe domain was maintained same as the mesh generated for single pipe simulation used
143 for single jet study; which has been established to be grid independent and validated with
144 experimental results. This gives us the confidence that the profile extracted from the pipe exit is
145 accurately predicting the flow physics. The mesh in the outlet of pipe domain is as shown in Figure
146 4. As with the previous study, the geometry was generated using SolidWorks, while the structured
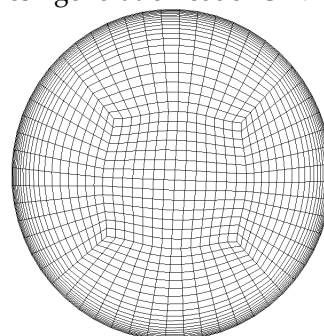147 mesh was created using proprietary mesh generation code ICEM-CFD.

Figure 4. Mesh at Pipe domain outlet

151   In order to ensure that accurate transfer of velocity and TKE data occurs from the pipe domain
152 to jet domain, it was necessary to maintain 1 to 1 grid connectivity between the pipe domain and the
153 domain downstream. Hence, the inlet of the jet domain (which acts as the exit of the pipe domain)
154 was very finely meshed, to maintain 1 to 1 grid connectivity. The grid generated near the pipe
155 exit/flow inlet section of jet domain is as shown in Figure 5. The band of very fine mesh elements seen
156 in the diagram corresponds to the wall surface mesh generated in the pipe domain. It is to be also
157 noted that the area between the jets are meshed with fine mesh to ensure that the flow physics due
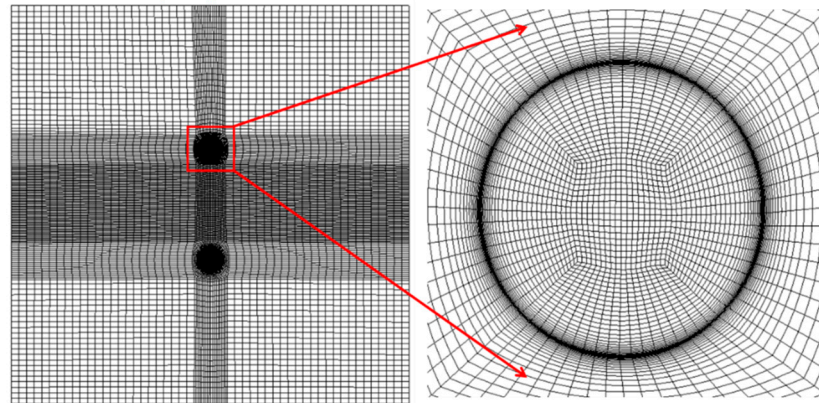158 to jet impingement is accurately captured.

159
160   **Figure 5.** Mesh near the jet domain inlet
161

162   The midplane showing the cut section of the mesh generated for the impingement domain is
163 shown in Figure 6. Care has been taken to ensure that the mesh extruding from the inlet section is
164 gradually growing towards the center to ideally capture the growth of the jets with sufficient
165 numerical accuracy. The spurious lines seen in the middle of the mesh is result of poor quality
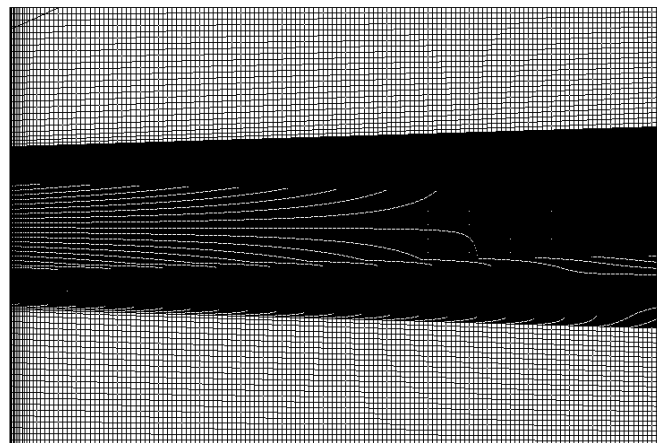166 graphical representation and not to be interpreted as any modification.

167
168   **Figure 6.** Mesh along center plane for full model jet domain

169 **4. Turbulence Model used**

170   The choice of turbulence model for the simulation of impinging jets is based on the work done
171 earlier on single jets [1]. Various turbulence models were analyzed for single jet flow conditions, and
172 it was found that SST k-ω model performed best for given range of Re under consideration. Hence,
173 for the current analysis, SST k-ω model was deemed as the best option in terms of turbulence models.
174 The details regarding SST k-ω model was discussed in [1].

175 **5. Boundary conditions and solver used**

176   The velocity and TKE profile extracted from the pipe exit is shown in Table 1 below. It is to be
177 noticed that three separate velocity components were used in this study (velocity u, v and w) instead
178 of single velocity profile (as used in single jet study) to ensure that all the appropriate velocity vectors

179   are transferred from the pipe domain into impinging jet domain. Velocity v is shown in negative
180   components since one of the pipe is pointed in negative y direction, while the other is pointed in
181   positive y direction.

182   **Table 1.** Velocity and TKE profile at exit of pipe domain
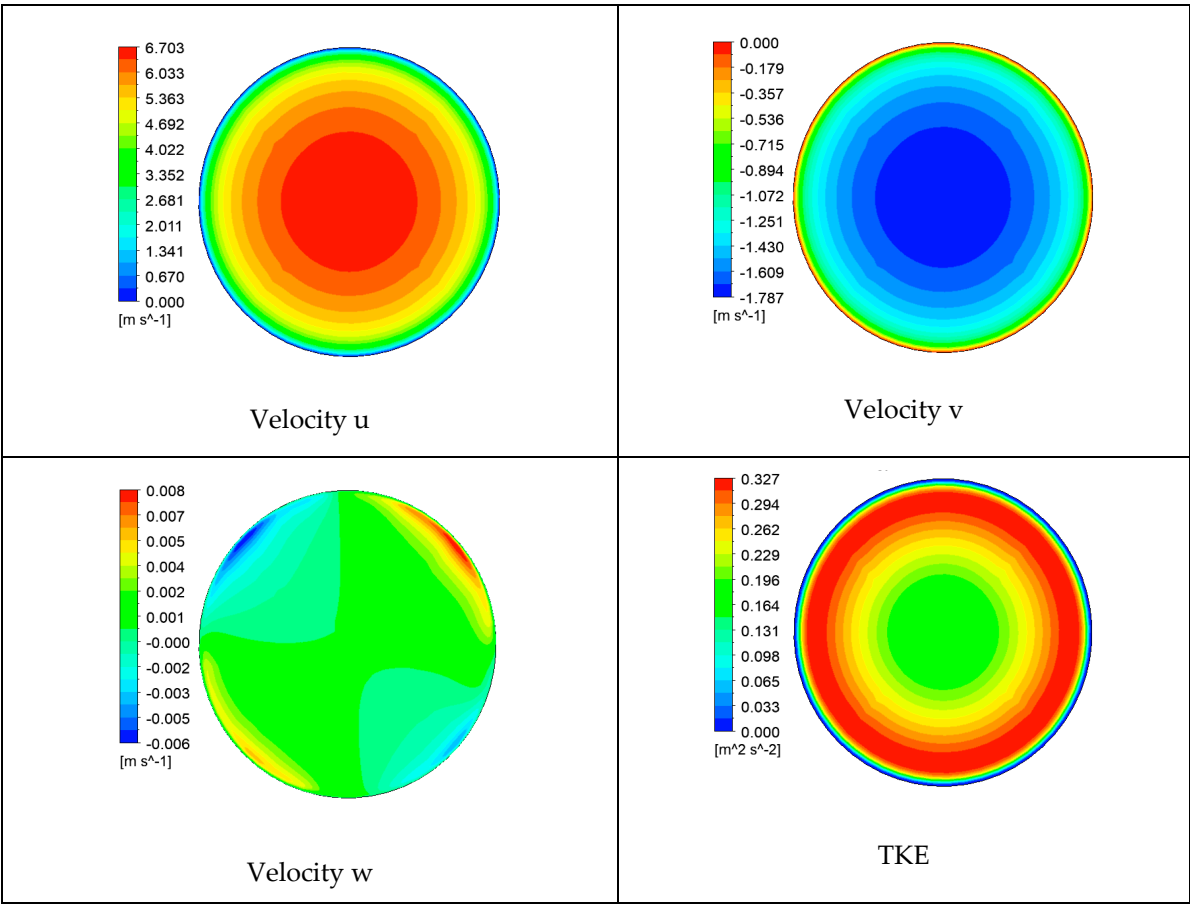
183
184   The schematic of boundary conditions used in the study is shown in the Figure 7 . The green
185   region denotes the inlet zone where pipe exit profile conditions are applied. The surface bounding
186   the inlets (shown in blue) are modelled as pressure outlet condition. This denotes a condition of
187   standard atmospheric pressure and temperature. This allows the flow to enter that surface in all
188   direction since pressure outlet condition in Ansys Fluent allows for backward flow. The side surfaces
189   of the domain (shown in white) are also modelled as pressure outlet conditions. This is necessary to
190   ensure that flow from all the direction is permitted to mix with the center jet flow, thereby ensuring
191   accurate physics of ambient air entrainment. The exit zone of the domain is also modelled as pressure
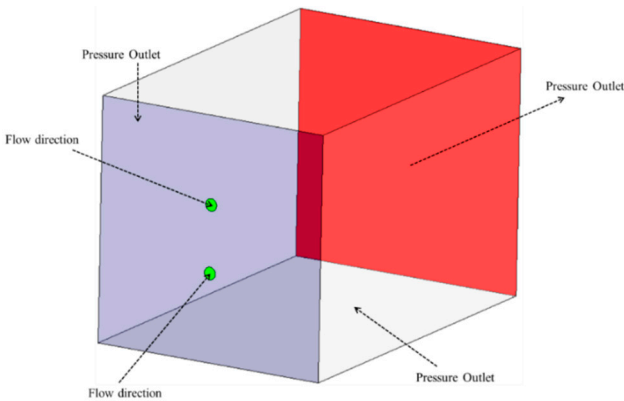192   outlet, thereby replicating a fully open surface for the jet to grow.
193

194
195   **Figure 7.** Schematic of boundary conditions used in the analysis

196
197　　　　The solver settings involved in this analysis is similar to that used in the case of single round jet
198　study [1]. SIMPLE algorithm was utilized for pressure-velocity coupling with the 2nd order Upwind
199　scheme used for spatial discretization. A convergence criterion of 10-6 was used for all the parameters
200　to confirm that the solution had fully converged with minimal numerical error. Once the residuals
201　for the convergence criterions were satisfied, the run was stopped, and the result files extracted to be
202　post processed.

203　**6. False diffusion study**

204　　　　One of the major concerns involved in the meshing of impinging jet domain was that the same
205　meshing philosophy used for single jet domain could not be used. In case of single jet, a single O-grid
206　exiting the pipe domain was extruded into the jet domain, which radially expanded outwards;
207　thereby capturing the relevant flow physics. In the case of impinging jets, there would be two such
208　O-grids which need to interact with each other (at the point of impingement). But it is not possible to
209　generate two (2) intersecting O-grids, as the mesh cannot overlap with each other. This lead us to the
210　conclusion that the only possible solution is to keep the O-grid mesh straight out of the pipe domain
211　parallel to the central plane, without any alignment towards the flow direction. This would require
212　the region between the impinging jets to be finely meshed in order to capture the all flow details with
213　the necessary precision.
214　　　　One of the major drawbacks of this approach is known to be False diffusion (FD). FD is defined
215　as the artificial diffusion introduced by the numerical scheme when the flow has predefined obliquity
216　to the grid lines and there exists a non-zero gradient of flow variables in the direction normal to flow.
217　It is a multi-dimensional phenomenon usually observed in cases with large Peclet number. FD was
218　extensively studied by de Vahl Davis and Mallinson [15] who proposed an approximation expression
219　to represent it in two-dimensional state as shown in equation below.
220

$$\Gamma_{False} = \frac{\rho * U * \Delta x * \Delta y * \sin 2\theta}{4(\Delta y * sin^3 \theta + \Delta x * cos^3 \theta)} \tag{1}$$

222
223　　　　The parameters used in equation 1 is defined in Table 2. Suhas Patankar [16] has provided a very
224　clear discussion of the issues related with FD in his book. He helps draw attention to the fact that:
225　　　　● FD manifests only when a mesh obliquity exists with respect to velocity profile.
226　　　　● FD becomes maximum when $\sin 2\theta$ is maximum, which is attained when θ becomes 45
227　　　　　degrees i.e. flow direction is at 45o to the grid alignment.
228　　　　● FD can be reduced by mesh refinement, i.e. having smaller values for Δx and Δy
229　　　　　respectively.
230　　　　● FD cannot be removed by using Central difference scheme, since Central difference
231　　　　　scheme are prone to produce unrealistic results at large grid Peclet number.
232
233　　　　　　　　**Table 2.** Explanation of parameters used in False Diffusion equation

Symbols	Parameters
Γ_{False}	False Diffusion Coefficient
ϱ	Density of the fluid
U	Average velocity of flow
Δx	Mesh size in x-direction

Δy	Mesh size in y-direction
θ	Angle made by the velocity vector with x-direction

234

235   This information highlighted the importance of choosing an appropriate numerical scheme for
236   the study. The work done by Raithby [17] and [18] provides insight into the research that has
237   undergone in gaining an understanding of this numerical phenomenon. Along the same lines, the
238   work done by Patel et al. [19] and [20] has suggested an updated numerical scheme which suffers less
239   from FD issues. Recent works (as of 2012) by Karadimou [21] show that there is still significant
240   interest in this aspect of numerical schemes.
241   Focusing our attention to the problem of jet impingement, where predetermined obliquity
242   between the velocity vector and grid direction exist; it was considered important to establish the effect
243   of FD in the prediction of velocity profiles. A qualitative and quantitative representation of this
244   numerical issue was necessary before proceeding with impingement jet study. Hence, it was decided
245   that a single jet case will be studied where the mesh is mis-aligned with the incoming velocity vector
246   and the results were compared with straight jet (where the mesh and velocity vectors are aligned)
247   result. The validation of straight round jet results with experimental data [1] has provided us with
248   confidence in the accuracy of those results, and hence they can be used as baseline data for future
249   validation.
250   For the study with misaligned flow, a domain similar to single jet study was designed as shown
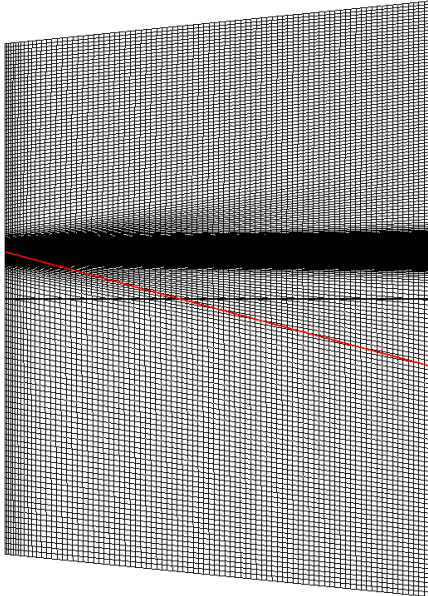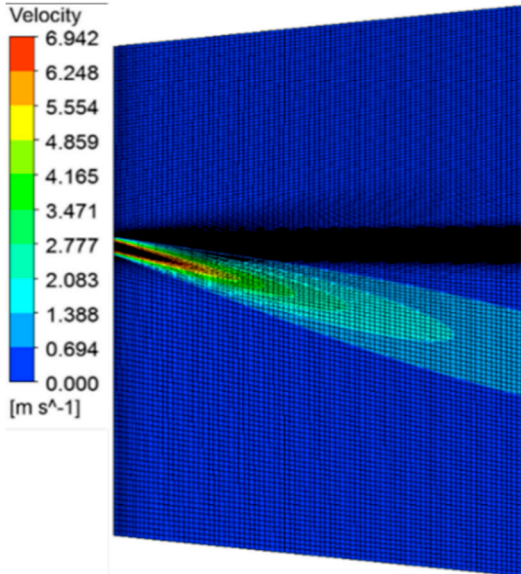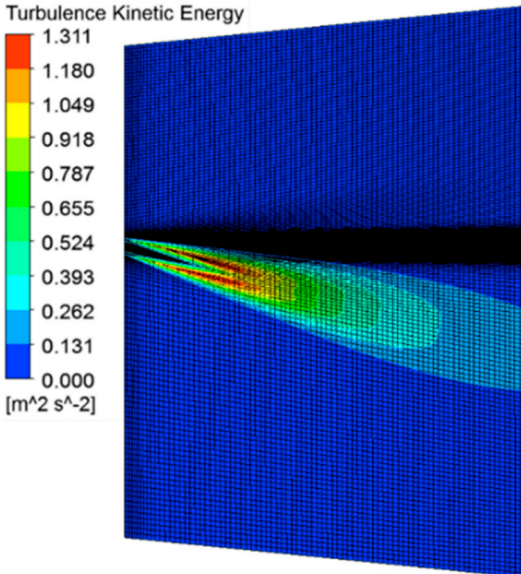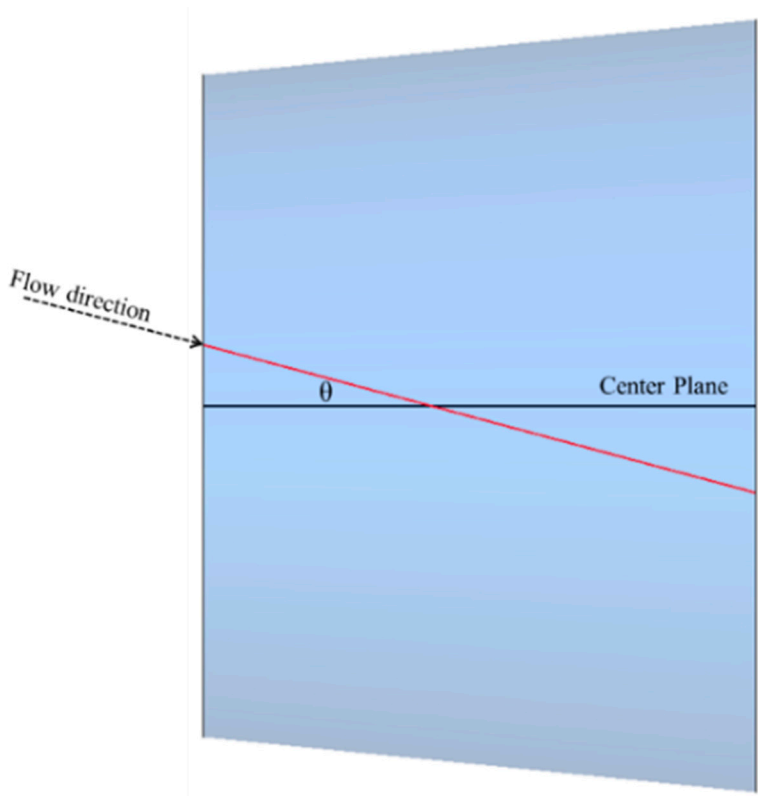251   in Figure 8.
252

253
254   **Figure 8.** Schematic of flow setup used for False Diffusion study
255

256   For this study, a mesh obliquity (θ) of 15o angle was considered. The center line of the flow is
257   shown in red color while the center plane to which the mesh is parallel is shown in black. The mesh
258   generated for the study is shown in table below. The node count used is exactly same as the node
259   count for mesh generated for straight jet flow. The velocity and TKE contour from study was
260   generated and overlaid with the mesh as shown in the table.

261

Table 3. Mesh generated for the study and velocity and TKE results

Mesh for flow setup

Velocity profile for case with misaligned mesh	TKE profile for case with misaligned mesh

262

263   For obtaining a clear understanding of the effect of mesh obliquity, velocity profile along the
264 center line of the flow was taken for consideration. From the study of single jet in [1], it was
265 established that none of the turbulence models used were capable of predicting the TKE parameter
266 with much accuracy beyond a distance of 6D from the pipe exit for the current range of Re studied.
267 Hence, for the impingement jet study, TKE parameter was not considered as a factor of special
268 interest and only velocity data was closely analyzed. Still, in the spirit of research interest; TKE
269 parameter was also plotted for the misaligned jet study and compared with straight jet data. The
270 velocity and TKE profile along the center line is shown in Table 4. It is observed that there exists a
271 difference in value for velocity and TKE along the center line for misaligned jet when compared to
272 straight jet. In case of velocity profile, this difference corresponds to 4.8% where as in TKE data, the
273 difference is approximately 63.5%.

274   **Table 4.** Velocity and TKE profile along the center line for straight and inclined jet (initial
275   mesh)
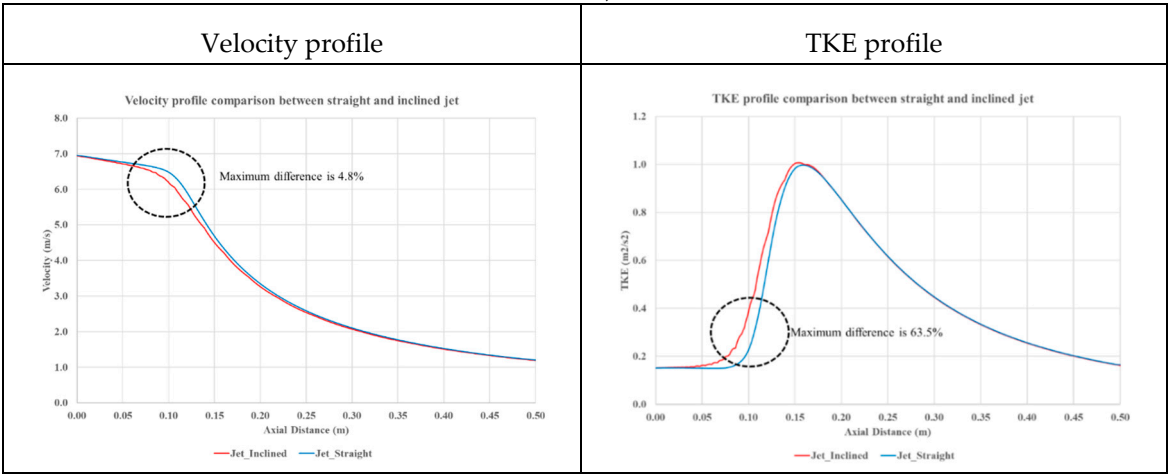
277   Even with using the same mesh that was used for straight jet, a considerable difference in the
278   value of velocity data was observed.   This indicates that numerical scheme applied in the
279   commercial CFD solver suffers from FD. It was decided that a refined mesh was to be tested to see
280   the impact of mesh size on the FD parameter.
281   Instead of generating a mesh with higher node count for the same domain size, the domain size
282   was brought down to half the initial size and the mesh count maintained the same; thereby ideally
283   reducing the Δx and Δy to approximately half of the initial value. The new generated mesh overlaid
284   with previous mesh is shown in Figure 9. The yellow line represents the 10.33D location from the
285   pipe exit which based on the centerline of the pipe identifies the impingement point.
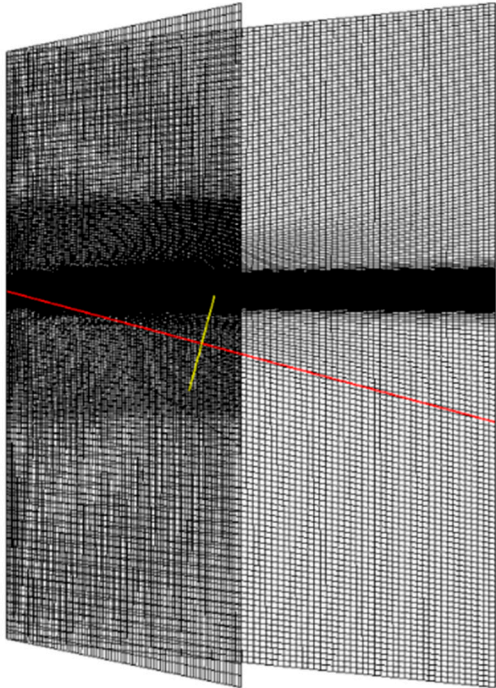

287   **Figure 9.** Refined mesh vs initial mesh generated for false diffusion study

289   Based on the refined mesh, CFD analysis was performed on the inclined jet flow and the results
290   compared to the results from previous mesh and straight mesh study. Again, the velocity and TKE
291   parameters were plotted along the center line and data compared with each other as shown in Table
292   5. The difference in TKE values dropped from 63.5% to 33% whereas the velocity difference had been
293   reduced from 4.8% to 3%. A mesh refinement by a factor of 2 has only reduced the difference in
294   velocity values by a margin of 1.8%; whereas significantly affected the TKE parameter.

295   **Table 5.** Velocity and TKE profile along the center line for straight and inclined jet (refined mesh)

Velocity profile	TKE profile

296
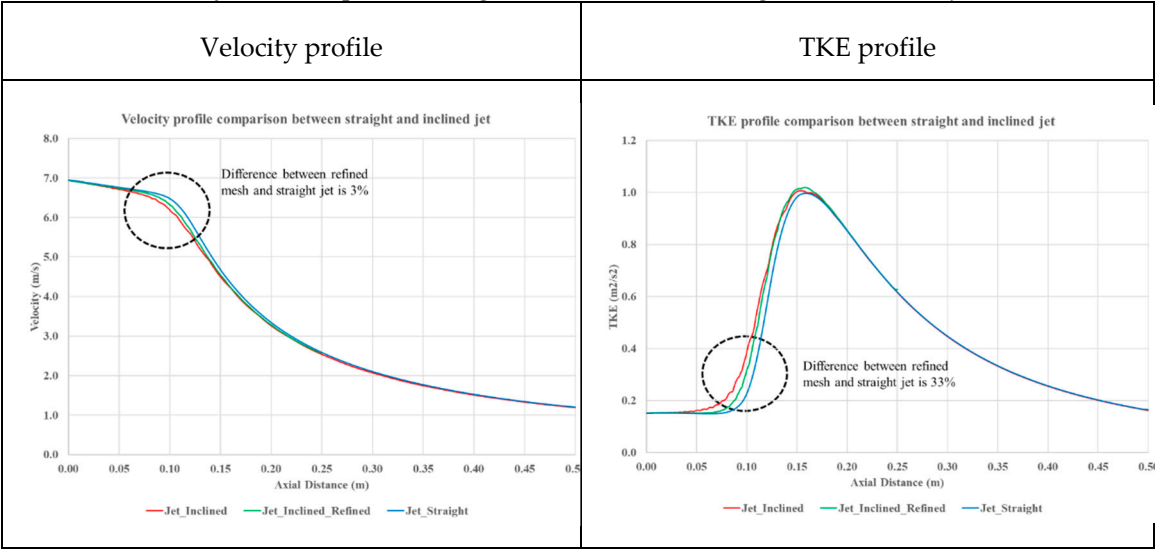
297   This implied that, if the domain size similar to single jet domain was to be used; a significantly
298   larger mesh size would be required to generate velocity data with the same accuracy. Hence, it was
299   deemed necessary that the domain size used for the jet impingement study be reduced by a
300   considerable margin so that high quality mesh can be generated at similar node counts. The
301   dimensions hence used for the domain in case of impingement jet study as (shown in Figure 3) can
302   be seen to be significantly smaller than the dimensions used for single jet study. This reduction in
303   domain size has helped us to efficiently allocate the nodes to the areas of higher interest without any
304   significant increase in node count. Care has been taken to ensure that the reduction in domain
305   dimensions did not affect any simulation physics.

306   **7. Full model vs Symmetry model**

307   Another major step considered to ensure that accurate flow results were obtained at minimal
308   usage of computational resources was to study the flow using full model (as shown in Figure 6) and
309   compare it with the results obtained from the symmetry based model (as shown in Figure 10). Since
310   the boundary conditions are symmetric about the central plane, it can be assumed that the flow
311   physics beyond interaction point is also symmetric in a steady state solution. If the velocity data
312   obtained from full model and symmetric model is comparable, then it can be asserted with confidence
313   that the symmetric model can produce accurate results which captures the steady state flow physics
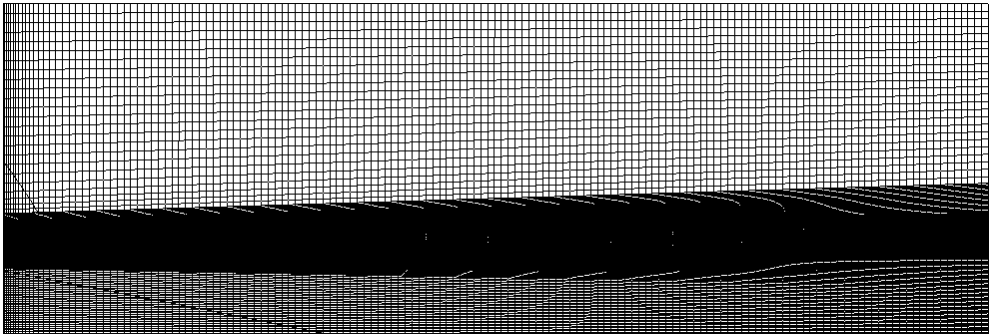314   completely.

315

316
317   **Figure 10.** Mesh along center plane for symmetry model jet domain
318

319   The region corresponding to the zone of impingement is very finely meshed as can be seen from
320   the picture above. The node count generated for the symmetric mesh is close to 1.35 million. Even
321   though, this value is very close to the mesh used for single jet study, it is to be considered that the

322   fluid domain used in the case of jet impingement study is significantly smaller, thereby ensuring
323   higher mesh density.
324   The planes where data was captured for the comparison is shown in the Figure 11. The naming
325   convention used by Landers [9] is followed in the current study. In the horizontal plane, the jet
326   impingement occurs at angle 2θ to one another. The impingement point lies on the intersection of
327   horizontal and vertical plane, at a distance of 10.33D from the pipe exit. The line formed at the
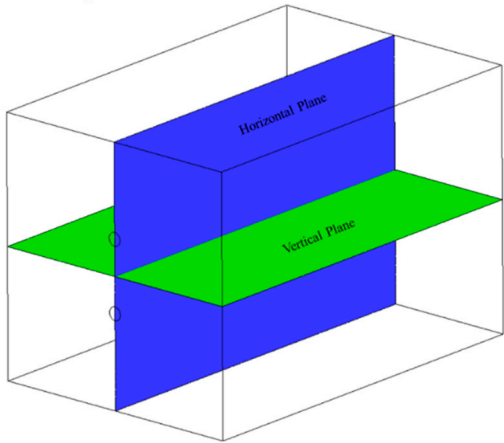328   intersection of horizontal and vertical plane is termed as the center line.

329
330   **Figure 11.** Location of planes used for the jet impingement study
331

332   To quantitatively compare the effect of symmetry model vs the full model for jet impingement
333   study, the center line velocity and TKE data was plotted and difference between them taken into
334   consideration. It was observed that the maximum difference in velocity value was close to 2.8%
335   whereas the maximum difference in TKE value was close to 2.3% as shown in Table 6. Since the
336   difference in values are negligible, it was concluded that using symmetry model for the jet
337   impingement study was an effective method to reduce the computational resource usage without
338   any major omission of flow physics.
339
340   **Table 6.** Velocity and TKE profile along the center line for full model and symmetry model

Velocity profile	TKE profile

341
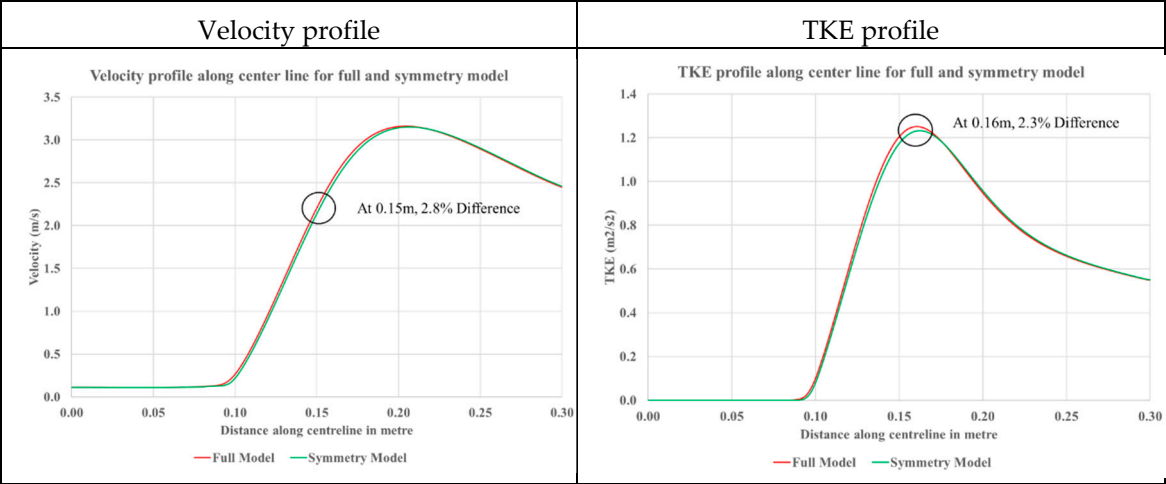
8. Grid Sensitivity study

343   For every independent CFD analysis performed, it needs to be carefully verified that the solution
344   was independent of the mesh count used by running the same simulation over various meshes and
345   finding the smallest mesh where the target parameter does not change significantly with the change
346   in mesh size.

347　　　　For the case of jet impingement study, the target parameter considered was velocity data along
348　　the center line at and beyond the impingement point. The velocity value at 10.33D and 12D along the
349　　center line was carefully noted for multiple meshes, and the general trend in variation was observed.
350　　The data was plotted systematically to identify the point of grid independence as shown in Figure
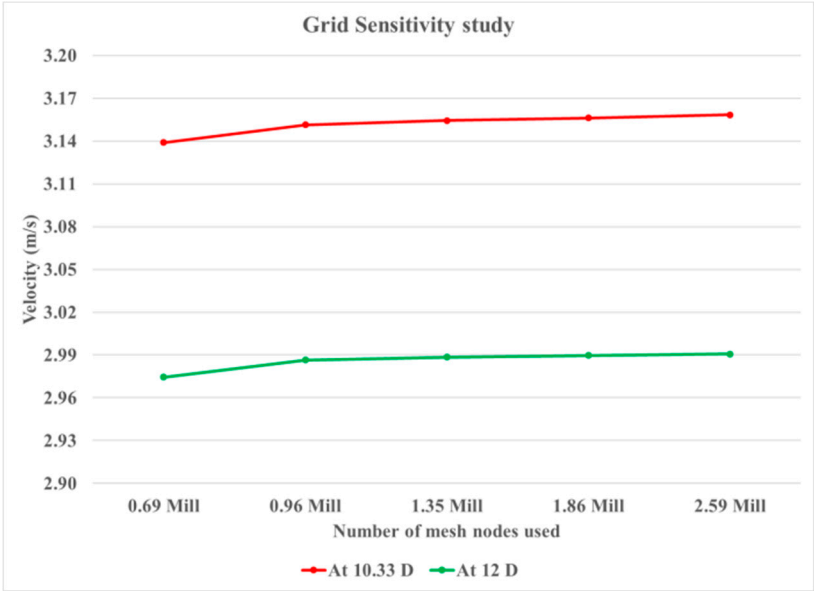351　　12.

352
353　　　　　　　　　　**Figure 12.** Grid sensitivity study performed for impinging jet domain
354

355　　　　From the above figure, it can be seen that the change in value of velocity is not significant when
356　　the mesh size is increase beyond 1.35 million nodes. Table 7 shows the magnitude of variation of
357　　velocity value for other meshes with respect to 1.35 million node case (which was considered to be
358　　the reference case). Since the relative change in value is seen to be small, the mesh with node count
359　　of 1.35 million nodes was considered as the point of grid independence.
360
361　　　　　　　　　　　　　　　　**Table 7.** Grid independence data

Node Count (millions)	At 10.33D along centerline			At 12D along centerline		
	Velocity (m/s)	Difference wrt Ref	% Difference wrt Ref	Velocity (m/s)	Difference wrt Ref	% Difference wrt Ref
0.69	3.139	0.015	0.488	2.975	0.014	0.468
0.96	3.151	0.003	0.095	2.986	0.002	0.072
1.35	3.154	0	0	2.989	0	0
1.86	3.156	-0.002	-0.057	2.990	-0.001	-0.037
2.59	3.158	-0.004	-0.124	2.991	-0.002	-0.072

362
363　　　　For all the further studies, a grid size of 1.35 million nodes was used with symmetric model for
364　　jet impingement domain. It is to be noted that with the study with different impingement angle, using
365　　the same grid size and meshing philosophy; changes in θ, Δx and Δy will occur; there by changing
366　　the values of FD per case basis. But, it has also been noted that the effect of FD is significantly less on
367　　velocity parameter when compared to TKE parameter. Hence, no significant difference between the
368　　simulated data and real physics is expected.

369　　**9. Effect of Impingement angle**

370　　　　After systematically attaining a grid size where the solution was found to be independent to
371　　further changes in the number of grid elements; 3 different cases with impingement angles of 30o,

372   45o and 60o at a Reynolds number of 7,500 were analyzed. Contours and data values were taken
373   along multiple planes to quantitatively and qualitatively understand the flow physics. The
374   experimental data from Landers [9] and Disimile et al. [2] has been used for validation of the CFD
375   data. This helps in providing confidence in the accuracy of computational results, and acts as the
376   stepping stone for further studies done on impinging jets.

377   *9.1. Velocity Profile validation*

378   Velocity data from Landers [9] was used to validate the simulation results to ensure that the data
379   obtained from simulation is of highest accuracy. Landers has provided non-dimensional velocity
380   profiles along horizontal and vertical planes, taken at different distances downstream of jet
381   impingement for all the jet impingement angles considered. Hence, the data extracted from [9] is
382   plotted against the data obtained from simulation.
383   The data from all the locations along horizontal plane are plotted together as shown in Table 8
384   below. It can be observed that the experimental data falls on a narrow band of values. But as the
385   impingement angle is increased, the spread in experimental data has increased as shown in case with
386   45 degree and 60 degrees. This may be due to the difficulties in accurately measuring of velocity
387   parameters when the flow field experiences high mixing.
388
389   **Table 8.** Non-dimensional velocity profile in horizontal plane for different impingement angle

390
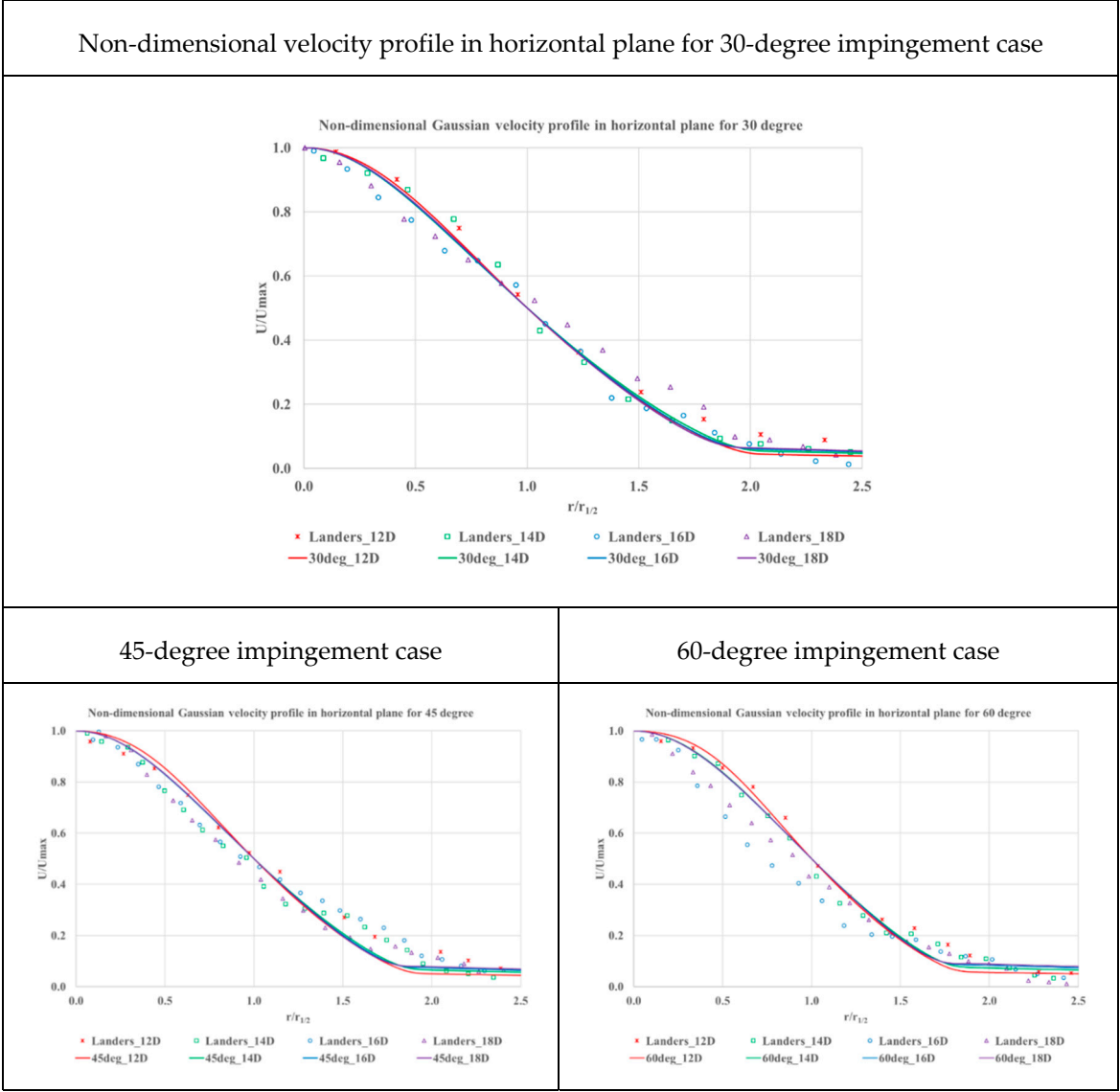
391 Similarly, data was extracted from vertical plane and plotted along multiple locations
392 downstream of jet impingement and compared with Landers's experimental data. In the vertical
393 plane, the data spread observed in the experimental results has increased as seen in Table 9. This can
394 possibly be attributed to problems during the experiment since the vertical plane witnesses higher
395 amount of jet interaction. Based on these validations, it was concluded that the results obtained from
396 simulations are of high quality, and further studies were conducted on the impinging jets.
397
398 **Table 9.** Non-dimensional velocity profile in vertical plane for different impingement angle

399 *9.2. Centerline Velocity Profile*

400 To quantitatively understand the difference in the flow characteristics of the resultant jet formed
401 from impingement at various angles, the velocity data along the centerline is taken. The center line
402 forms as the intersection of horizontal and vertical plane, thereby carrying the characteristics of both
403 the planes.
404 The velocity profile along the center line for 3 impingement angles are plotted as shown in Table
405 10 and compared with the single jet data. Beyond impingement point of 10.33D; the decay rate of
406 velocity along the center line of the resultant jet resembles the decay rate for the single jet. Also, it is
407 to be noted that the maximum velocity in the case of 30-degree impingement angle is higher than the
408 value observed in case of 60-degree impingement.

409   **Table 10.** Actual and normalized velocity profile along the center line for various impingement
410   angle

Actual velocity profile	Normalized velocity profile
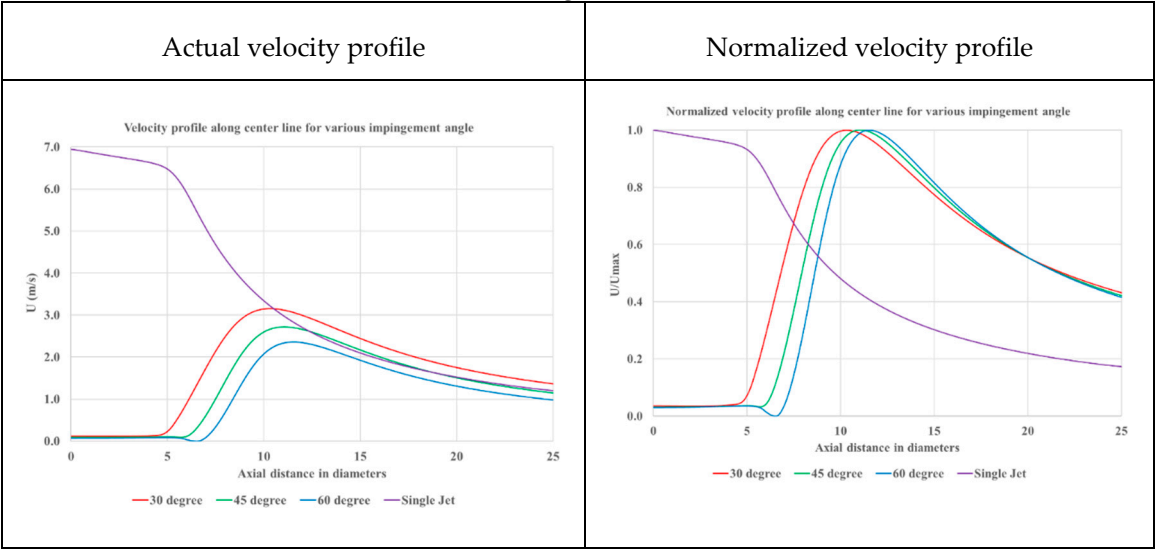
411
412   To further understand the decay physics, normalized velocity profile along the center line was
413   also plotted. From above figures shown in Table 10, it can be seen that the maximum velocity seen
414   along the center-line shifts downstream and moves beyond impingement point as the jet
415   impingement angle is increased. This effect can be explained to the fact that at higher impingement
416   angle, the individual jets have already spread significantly before reaching the point of interaction;
417   and hence carry lesser energy with them. The area of interaction between the jets has also increased
418   significantly due to higher spread of the jets; and hence the zone of higher velocity gets shifted
419   beyond the impingement zone.
420   The center-line decay of velocity for an axi-symmetric jet can be modelled with a 1/x decay
421   profile, where x represents the distance from the pipe exit. In Figure 13, a 1/x profile was generated
422   and plotted against single jet results showing that the single jet center line velocity decay obeys the
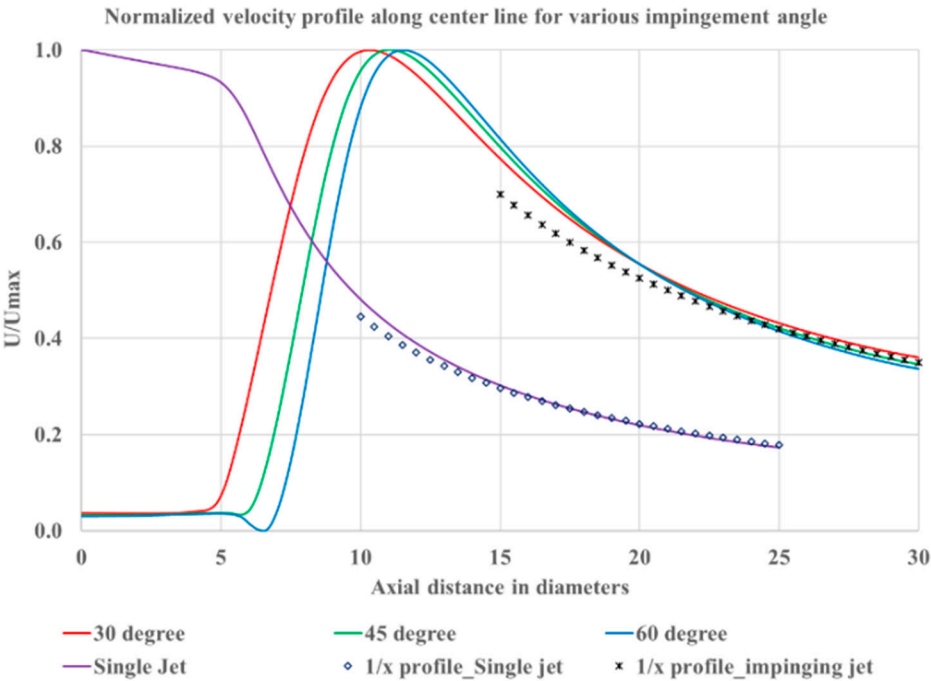423   1/x decay profile.

424
425   **Figure 13.** Normalized velocity profile along the center line compared with 1/x profile
426

427   Similarly, when 1/x profile was plotted for the resultant jet formed from jet impingement, it can
428   be seen that beyond 20D (almost 10D downstream of the jet impingement point); the resultant jet also
429   obeys a 1/x decay profile. This implies that at 10D from jet impingement point; the resultant jet formed
430   has the fully developed characteristics of a single jet and does not behave as 2 independent jets.

431   *9.3. Centerline TKE Profile*

432   The TKE profile along the center line for the 3 cases of impingement angle is plotted as shown
433   in figures in Table 11 and qualitatively compared with experimental data obtained by Landers [9].
434   From the single jet results, it was established that beyond 6D, the simulation overpredicted the TKE
435   parameters. In a qualitative sense, it was observed that the simulation followed the similar trend
436   observed in experimental data. Hence, only qualitative comparison with Landers' experimental
437   results was performed by using normalized parameters.
438   From Table 11, for 30-degree impingement case; it can be observed that the CFD results predict
439   the peak in TKE parameter almost 1.5D before the peak observed in experimental data. Also, the
440   experimental data shows a significantly sharper fall in TKE parameter compared to the results
441   obtained from the simulation.

442
443   **Table 11.** Normalized TKE profile along the center line for various jet impingement
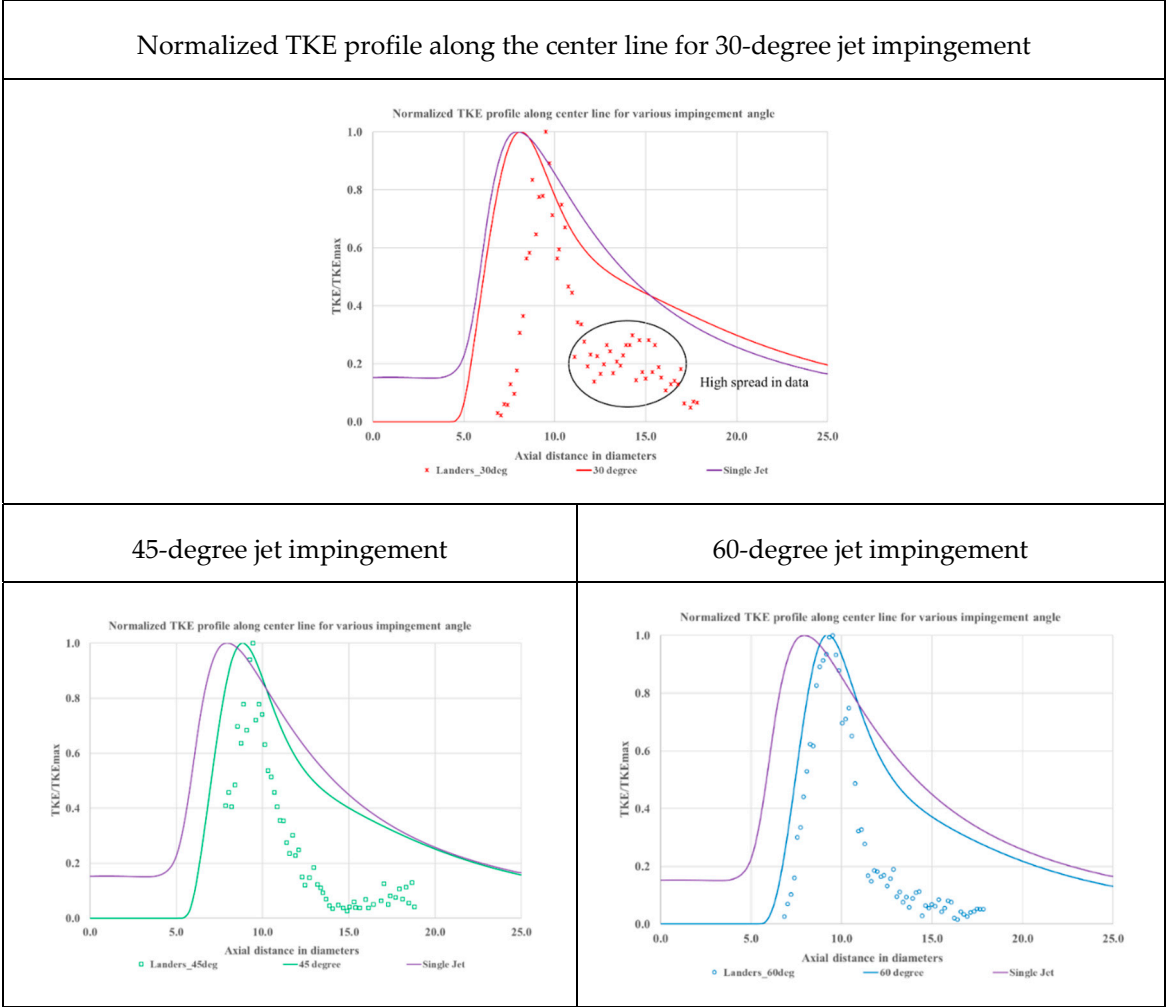
444
445   As the impingement angle is increased to 45 degrees, the difference in trend between the
446   experimental data and computational results is seen to have reduced. This can be observed above
447   where the peak in TKE obtained from experimental results and computational results are off by a
448   margin of 0.6D. Still, a significant difference in the post impingement TKE profile exists between
449   experimental and computational data.

450   With further increase in impingement angle to 60 degrees, the difference in trend between the
451 experimental data and computational results is seen to become negligible before impingement as
452 seen above. Both experimental and computational data predicts the zone of highest TKE at the same
453 location (almost 1D before impingement point). Beyond impingement point, the difference in TKE
454 value predicted by the experimental methodology significantly differs from the CFD results. It is to
455 be considered that the jet impingement leads to highly turbulent mixing regions where significant
456 interaction of turbulent scales occur. The turbulence model used in this steady state analysis may not
457 be able to account for the interaction and hence the significant difference in TKE values measured by
458 experiment and obtained from CFD simulation.
459   The data from all the different impingement angles is plotted together as shown in Figure 14 for
460 easier visualization. It can be seen the experimental data follows a very narrow band of values before
461 and after impingement (except for the spread in experimental data for the 30-degree case). At 5D
462 beyond impingement point, it can be observed that all the simulation data follows a similar trend,
463 with 30-degree case having higher normalized TKE when compared to 45 and 60-degree
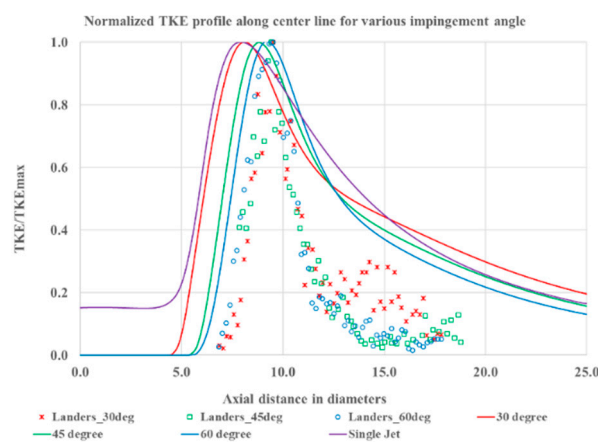464 impingement cases.

465
466   **Figure 14.** Normalized TKE profile along the center line for various angles of impingement
467

468   A better understanding of the turbulent properties can be attained by plotting the turbulence
469 intensity along the center-line as shown in **Error! Reference source not found.**. It can be observed
470 that the maximum turbulence intensity observed in the single round jet is 11.7%. In the case of 30-
471 degree impinging jets, this value goes up to 28.7% which denotes an increase in turbulence intensity
472 of 145%.
473   Between 30 and 45-degree case, the turbulence intensity increases from 28.7% to 34.7% which
474 represents an increase of 21%. And between 45 and 60-degree case, the turbulence intensity increases
475 from 34.7% to 40.5% signifying an increase of 17%. This implies that at higher impingement angle,
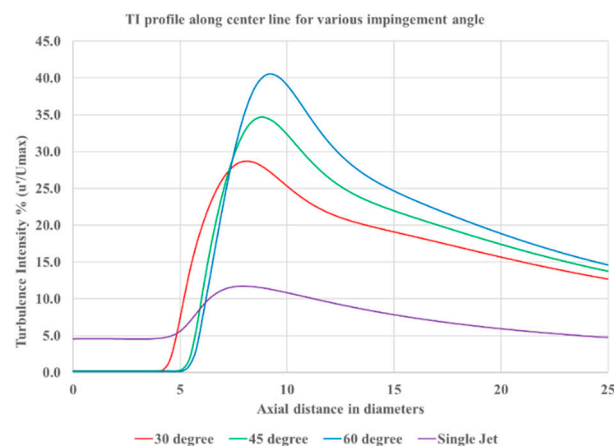476 we can expect higher turbulence intensity which will enhance near field mixing.
477

478
479   **Figure 15.** Turbulence intensity profile along center line for various angles of impingement

480   *9.4. Spread profile of the jet*

481   To estimate the spread profile of the jet in horizontal and vertical planes, velocity values were
482   considered along radial locations for every 10 degrees at 3 locations downstream of jet impingement
483   point; at 12D, 16D and 20D beyond pipe exit. Along these radial locations, the velocity values were
484   calculated to estimate the half-width. Half-width is defined as the location along the line where the
485   velocity becomes half of the center-line velocity. Using the half-width half-max (HWHM) as the
486   measuring parameter, the profile of the jet at that plane was plotted. It is interesting to observe that
487   the jet attains an elliptical profile after impingement as shown in Table 12. The half width along the
488   radial lines was normalized using pipe diameter. A similar observation was made by Disimile et al.
489   [2] and Rho et al. [3]. This provides confidence in the legitimacy of the results and act as a validation
490   criterion. Similarly, jet profile was analyzed at various locations for the 45-degree and 60-degree case.
491   The results from the analysis is shown above. From these 3 figures, it can be observed that the growth
492   of jet in z direction (in vertical plane) is significantly higher when compared to the growth in y
493   direction (in horizontal plane).
494
495   **Table 12.** Profiles of jet after impingement at different angle at various locations
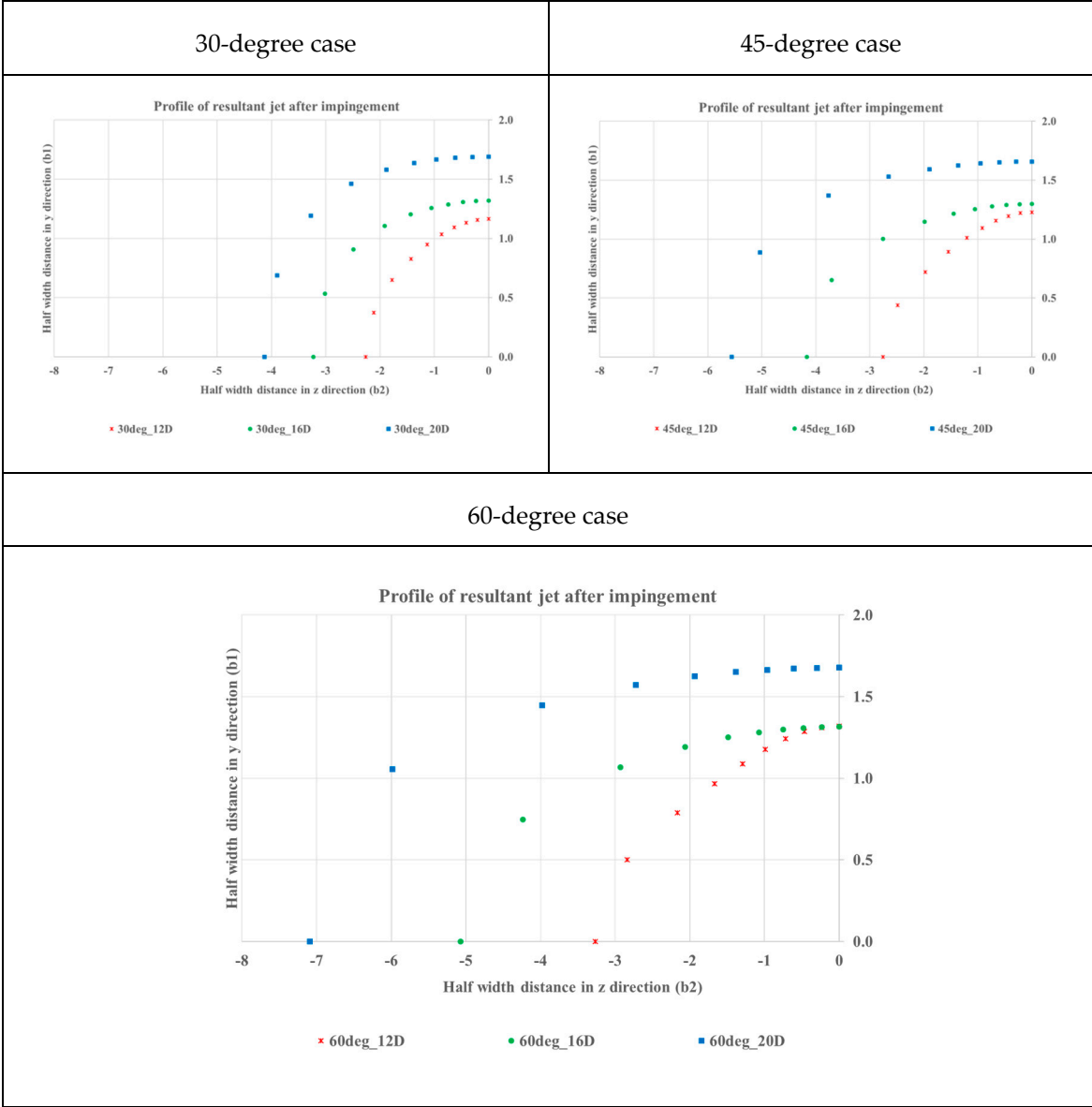
496
497   Interestingly, it was observed that for all the impingement angles; the half distance in y direction
498   reaches a maximum value for any given location beyond 12D and does not change significantly with

499 impingement angle. For example, the b1 parameter (half distance in y direction normalized with
500 diameter of pipe) is approximately 1.3 for all the cases at 16D from pipe exit and 1.7 for all cases at
501 20D. This is clearly represented in Table 13 below. Even though the spread in y direction is not
502 affected by the impingement angle, the growth of the jet in z-direction shows promising results. With
503 the increase in in impingement angle, the growth in z-direction increases as we move further
504 downstream.
505
506   **Table 13.** Profiles of jet at various locations after impingement at different angle
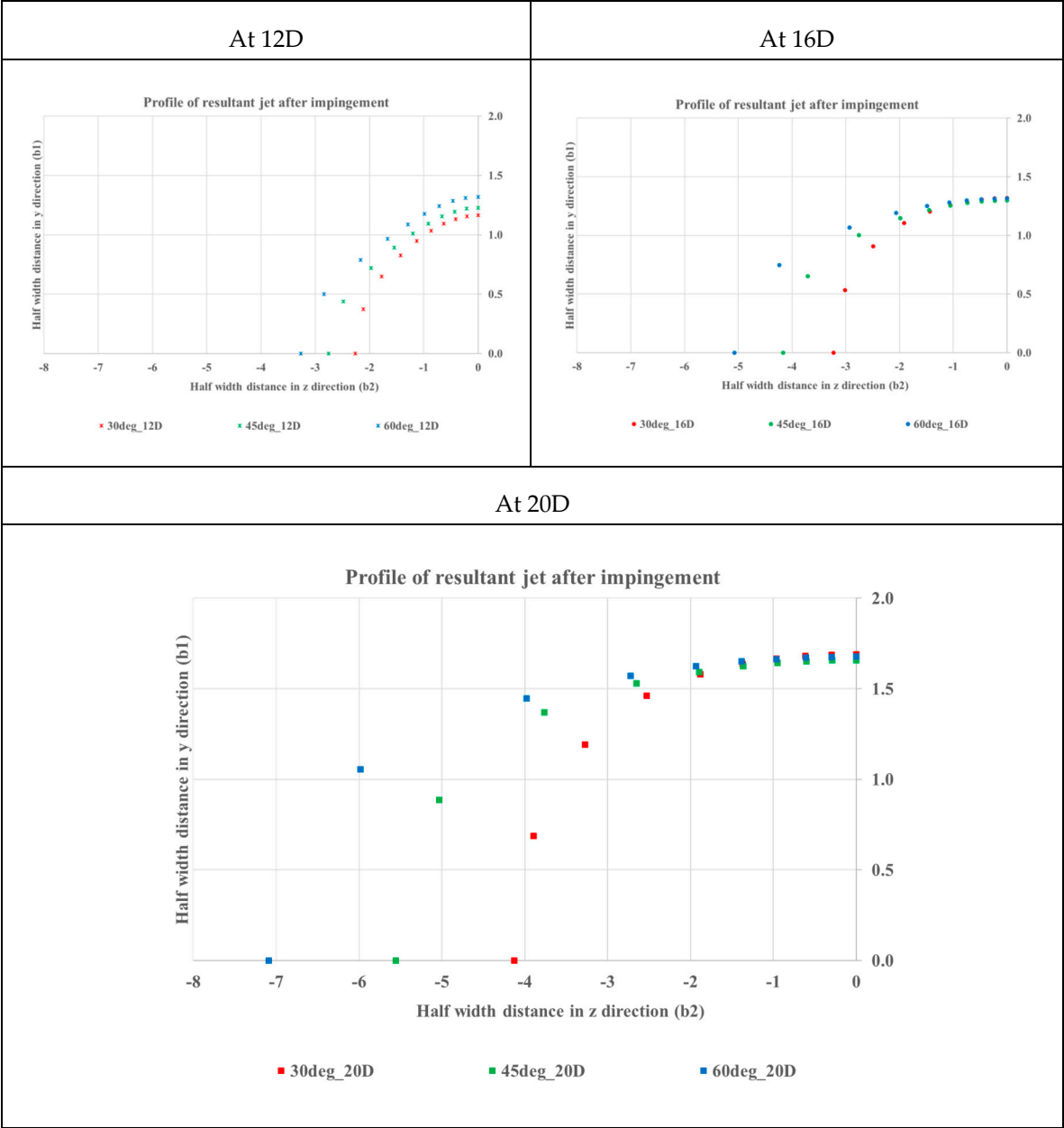
507
508   The data regarding the growth of the jet in y and z direction is represented using parameters b1
509 and b2; where b1 is the half width along the y direction measured in pipe diameters and b2 is the half
510 width along the z direction. The data is shown in Table 14, where the growth along y and z directions
511 are normalized to show the effect of location and angle on growth along the planes. The parameter
512 b2/b1 represents the ratio of growth in vertical plane to growth in horizontal plane. For a round jet,
513 the value of b2/b1 is 1 at every location.
514   From the below table we can conclude that the growth at 20D in vertical plane achieved by jets
515 impinging at 30-degree angle can be achieved by 16D by 45-degree impinging jets and approximately
516 at 14D by 60-degree impinging jets.

517   **Table 14.** Growth profile of resultant jet in y and z direction

| Case	Location	b1	b2	b2/b1
30-degree Impingement	12D	1.17	2.26	1.94
	16D	1.32	3.23	2.45
	20D	1.69	4.13	2.44
45-degree Impingement	12D	1.23	2.76	2.24
	16D	1.30	4.17	3.21
	20D	1.66	5.56	3.35
60-degree Impingement	12D	1.32	3.26	2.47
	16D	1.32	5.07	3.86
	20D	1.68	7.09	4.23

518
519   Growth profile along all the location for the 3 impingement angle cases are plotted as shown in
520   figures in Table 15. It is observed that at impingement angles of 30-degree, the profile at 12D matches
521   with the elliptical profile; but doesn't tend to match at 20D. But at case with higher impingement
522   angle of 60-degree, the further downstream locations have better match than the upstream location.
523   In all the cases, the computed profile closely follows an elliptical shape at 16D location. For the case
524   with 60-degree impingement angle, we can observe a strong deviation from the elliptical profile at
525   12D. This may be caused by the intense interaction between fluid streams which accounts for further
526   developing profile.
527
528   **Table 15.** Comparison of velocity profile with elliptical profile at different impingement angles
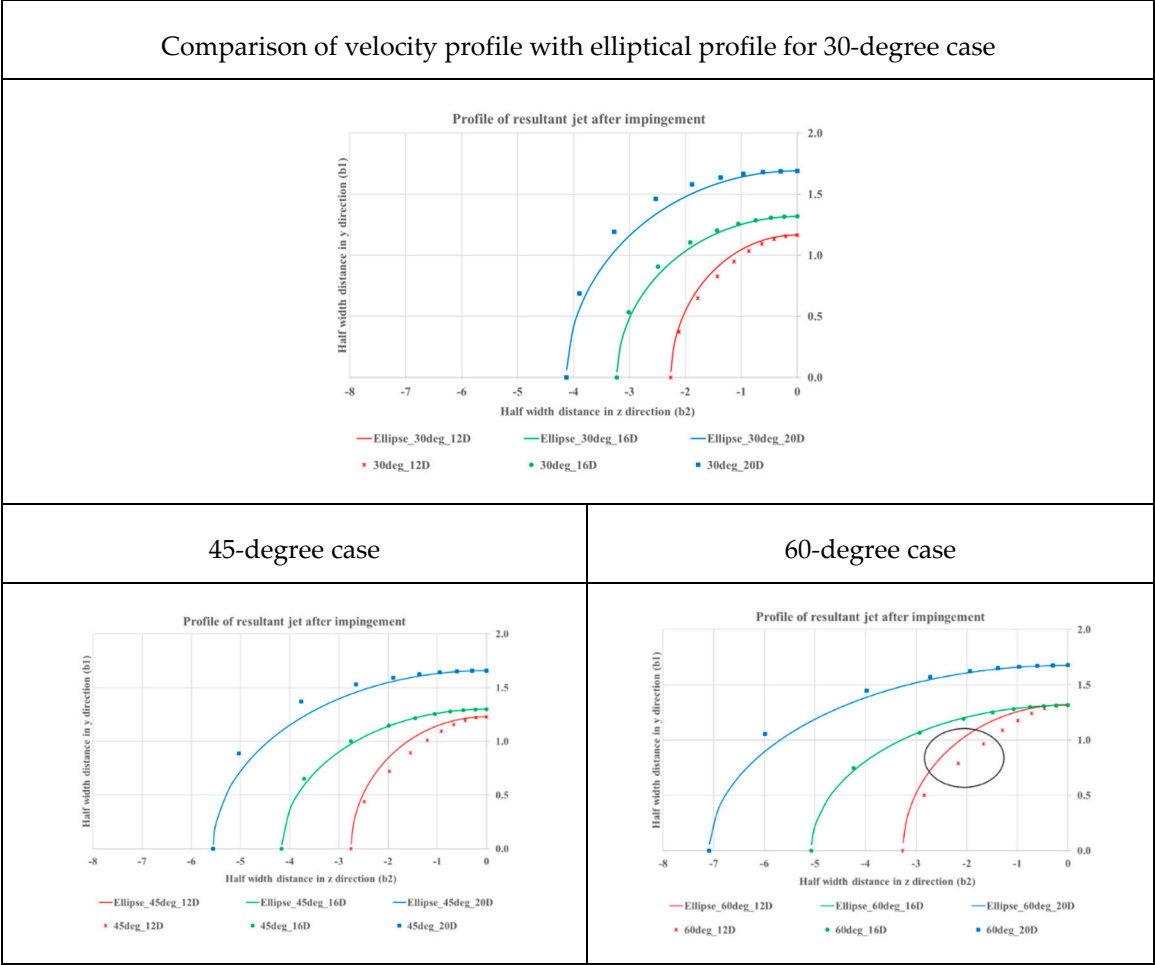
529

10. Conclusion

From the current study of jet impingement at constant angle and constant Reynolds number, the following conclusions were made based on the validated computational results.

1.   SST k-ω model can predict velocity characteristics of impinging jets with high level of accuracy but may not be suitable for predicting TKE parameters at low Reynolds number.

2.   The mesh obliquity with the velocity vector has an adverse effect on the numerical solution obtained and is referred to as False Diffusion (FD).

3.   FD increases with the increase in velocity, mesh oblique angle and the mesh size in all directions.

4.   The only possible method to reduce false diffusion for any given set of boundary conditions is to minimize mesh size by maximizing node count; which will be computationally expensive.

5.   Symmetry models, when compared to full domain models are equally capable of predicting the flow physics arising from jet impingement.

6.   For the study with different jet impingement angles, the velocity data obtained from computational analysis was validated with experimental data from [9].

7.   The Gaussian non-dimensionalized velocity profile matches with experimental data for all impingement angles in both horizontal and vertical planes.

8.   Region of higher velocity along the center-line was observed to shift beyond impingement point at higher values of impingement angles.

9.   The resultant jet formed from the jet interaction obeys 1/x profile of jet center-line velocity decay suggesting that the combined flow takes on the character of a single circular jet.

10.   Normalized TKE profile matches with experimental data at higher impingement angle and does not seem to agree well with experimental result at lower impingement angle.

11.   The resultant jet follows an elliptical profile beyond impingement point.

12.   The growth of the jet along the plane perpendicular to the plane of the jet is significantly higher than the growth along the pipe plane.

13.   The growth profile in both the planes is dependent on the impingement angle.

Author Contributions: Investigation, R.N.G; Supervision, P.J.D.

Conflicts of Interest: The authors declare no conflict of interest.

Nomenclature

CFD – Computational Fluid Dynamics

Re – Reynolds Number

TKE – Turbulence Kinetic Energy

TI – Turbulence Intensity

SIMPLE - Semi-Implicit Method for Pressure Linked Equations

FD – False Diffusion

HIA – Half Impingement Angle

FIA – Full Impingement Angle

b1 – half width of jet in plane of pipe

b2 – half width of jet in plane perpendicular to the plane of pipe

HWHM- Half width at the half Maximum

D – Diameter of pipe (mm)

θ - Half impingement angle (degrees)

k – Turbulent kinetic energy (m2/s2)

ω – Specific Dissipation rate (1/s)

578   $r_{1/2}$ – Jet Half width (m)

579   Γ_{false} – False diffusion coefficient

580   ϱ – Density of fluid

581   U – Average velocity of the flow

582   Δx – Mesh size in x-direction

583   Δy -Mesh size in y-direction

584   θ – Angle made by velocity vector with x-axis

585   **Reference**

586   1.   R. N. Gopalakrishnan and P. J. Disimile, "Effect of Turbulence Model in Numerical Simulation of Single
587   Round Jet at Low Reynolds Number," International Journal of Computational Engineering Research, vol.
588   7, no. 3, 2017.
589   2.   P. Disimile, E. Savory and N. Toy, "Mixing characteristics of twin impinging circular jets," Journal of
590   Propulsion and Power, vol. 11, no. 6, 1995.
591   3.   B. J. Rho, J. K. Kim and H. A. Dwyer, "Experimental study of a turbulent cross jet," AIAA Journal, vol. 28,
592   no. 5, 1988.
593   4.   "F-1 ENGINE INJECTOR," Heroic Relics, [Online]. Available: http://heroicrelics.org/info/f-1/f-1-
594   injector.html.
595   5.   B. D. Landers and P. J. Disimile, "Near Field Measurements of an Axisymmetric Turbulent Jet at Low
596   Reynolds Numbers: A PIV and CTA Comparison," nternational Journal on Theoretical and Applied
597   Research in Mechanical Engineering (IJTARME), vol. 4, no. 4, 2015.
598   6.   B. D. Landers and P. J. Disimile, "Passing Frequency of Vortical Structures in the Near Field of an
599   Axisymmetric Turbulent Jet," SSRG International Journal of Mechanical Engineering (SSRG-IJME), vol. 2,
600   no. 10, 2015.
601   7.   B. D. Landers and P. J. Disimile, "The Growth Characteristics of Transient Impinging Axisymmetric
602   Turbulent Jets," Journal of Flow Visualization and Image Processing, vol. 21, no. 1, 2016.
603   8.   B. D. Landers, P. J. Disimile and P. R. Snow, "The growth characteristics of a starting axisymmetric turbulent
604   jet," Journal of Visualization, 2016.
605   9.   B. D. Landers, "Mixing characteristics of turbulent twin impinging axisymmetric jets at various
606   impingement angles," 2016.
607   10. N. Rajaratnam, Turbulent Jets, Elsevier, 1976.
608   11. N. Rajaratnam and A. Khan, "Intersecting circular turbulent jets," Journal of hydraulic research, vol. 30,
609   1992.
610   12. N. Rajaratnam and S. Wu, "Intersecting circular jets of unequal momentum flux," Journal of hydraulic
611   research, vol. 30, 1992.
612   13. S. Elangovan, A. Solaiappan and E. Rathakrishnan, "Studies on twin non-parallel unventilated
613   axisymmetric jets," Proc lnstn Mech Engrs, vol. 210, 1996.
614   14. S. Elangovan, A. Solaiappan and E. Rathakrishnan, "Studies on twin non-parallel unventilated high-speed
615   jets," Proc lnstn Mech Engrs, vol. 211, 1997.
616   15. G. de Vahl Davis and G. Mallinson, "False diffusion in numerical fluid mechanics," 1972.
617   16. S. Patankar, Numerical Heat Transfer and Fluid FLow, 2013.
618   17. G. Raithby, "A critical evaluation of upstream differencing applied to problems involving fluid flow,"
619   Computer Methods In Applied Mechanics And Engineering, vol. 9, 1976.
620   18. G. Raithby, "Skew upstream differencing schemes for problems involving fluid flow," Computer Methods
621   In Applied Mechanics And Engineering, vol. 9, 1976.
622   19. M. Patel, M. Cross and N. Markatos, "Method of reducing false-diffusion errors in convection-diffusion
623   problems," Appl. Math. Modelling, vol. 9, 1985.
624   20. M. Patel, M. Cross and N. Markatos, "An assessment of flow-oriented schemes for reducing false diffusion,"
625   International Journal For Numerical Methods In Engineer, vol. 26, 1988.
626   21. D. Karadimou and N. Markatos, "A novel flow-oriented discretization scheme for reducing false diffusion
627   in three dimensional (3D) flows: An application in the indoor environment," Atmospheric Environment,
628   vol. 61, 2012